TECHNICAL REPORT

Title: Simulations of Target Acquisition with MIRI Four-Quadrant Phase Mask Coronagraph (IV): Predicted Performances Based on Slew Accuracy Estimates	Doc #: JWST-STScI-003712, SM-12 Date: 24 February 2014 Rev: -
Authors: Charles-Philippe Lajoie, Rémi Soummer, Dean C. Hines, & The JWST Coronagraphs Working Group — Phone: 410 - 338 - 5007	Release Date: 2 June 2014

1 Abstract

We report updated results from our latest set of simulations of target acquisition for MIRI's four-quadrant phase mask (4QPM) coronagraphs and provide a summary overview of our work based on various estimates for the observatory slew accuracy, for each of the MIRI coronagraphs. We use three different slew accuracy models and determine the optimal target acquisition scenario as well as estimated contrast performance for the 4QPM coronagraphs at 10.65 μm, 11.40 μm, and 15.50 μm. In general, fewer slews lead to more accurate final pointings, so we favor the scenario with a single target acquisition (Single TA). We find that the best contrast at any coronagraph wavelength is achieved with the most recent estimate (and most optimistic) model for the small angle maneuver (SAM) accuracy. However, background photon noise might limit further the contrast especially for fainter targets and the longer wavelengths. The main goal of this report is to provide a concise summary of all our simulations with an emphasis on the expected performances at different wavelengths based on the observatory slew accuracy.

2 Introduction

The achievable performance of the MIRI four-quadrant phase masks (4QPM) depends strongly on the observatory slew accuracy. In previous reports (Lajoie et al. 2012, 2013), we investigated various target acquisition methods aimed at minimizing the adverse effects of the 4QPM and slew accuracy on target acquisition. We used three different slew accuracy models, shown in Figure 1, and determined the performances of target acquisition for each of them. More recently, we also investigated the impact of various slew accuracy models and latency on the contrast for the 4QPM at different wavelengths (Lajoie et al. 2013). We now summarize all our previous results and discuss the overall performances of MIRI TA under the same three pointing accuracy models: one based on the requirements (REQ), another based on the new expected slew accuracy (CDR), and an intermediate case (INT; see Figure 1). The most optimistic small angle maneuver (SAM) accuracy used in this report (5 mas, 1-sigma/axis) is consistent with current estimates of the performance at the time of this report from the January 2014 Spacecraft critical design review (S/C-CDR). The latest numbers we have are as follows:

- FOV Offsets - Small (0-0.5 arcsec) (MR-182, OBS-194)
  Requirement: 5.0 mas (1-sigma/axis)
  Allocated: 4.8 mas (1-sigma/axis)
  Calculated: 4.0 mas (1-sigma/axis)
- FOV Offsets - Medium (0.5 - 2.0 arcsec) (MR-181, OBS- 1685)
  Requirement: 20.0 mas (1-sigma/axis)
  Allocated: 10.4 mas (1-sigma/axis)
  Calculated: 4.2 mas (1-sigma/axis)
- FOV Offsets - Large (2-20 arcsec) (MR-374, OBS-193)
  Requirement: 20.0 mas (1-sigma/axis)
  Allocated: 14.6 mas (1-sigma/axis)
  Calculated: 4.6 mas (1-sigma/axis)

In general, the REQ and INT slew models bear significantly larger errors for large slews compared to the current expected models (CDR), which translates into degraded overall performance.

As for contrast performances, based on Cavarroc et al. (2008), a performance goal of the order of 2.5×10^{-5} at 10 λ/D was determined by the MIRI team (Hines & Rieke, priv. communication; see also Boccaletti et al. 2005, Cavarroc et al. 2008) to be adequate to achieve MIRI's coronagraphic primary science goals in the F1065C band. Note that there are no performance requirements at smaller inner working angles or at other wavelengths. The 11.4 and 15.5 4QPMs are actually background limited at 12 λ/D and 6 λ/D, respectively, while the 10.65 4QPM is not (as shown below and in Lajoie et al. 2013). This goal at 10.65 μm originates from the fact that circumstellar disks and host galaxies of Active Galactic Nuclei (AGN) are expected to be imaged at ~10 λ/D. This performance goal at 10 λ/D is also expected to allow for Jupiter-mass planets, which are typically located between 1-3 λ/D, to be imaged around Gyr old stars. The performance of the MIRI coronagraphs will allow astronomers to complement observations from various observations. For example, the Gemini Planet Imager and SPHERE instrument (Gemini South and VLT respectively) are expected to directly image many new Jupiter mass planets at 0.1" – 1.0" for the first time. Astronomers will want to follow these objects up using all three of the MIRI 4QPMs to search for absorption in the Ammonia (NH_3) band at 10.65 μm, and to measure the adjacent continuum at 11.4 μm and the longer wavelength continuum at 15.5 μm. It is therefore essential to assess the performance of the MIRI coronagraphs and to determine the level of contrast one can expect at different angular separations.

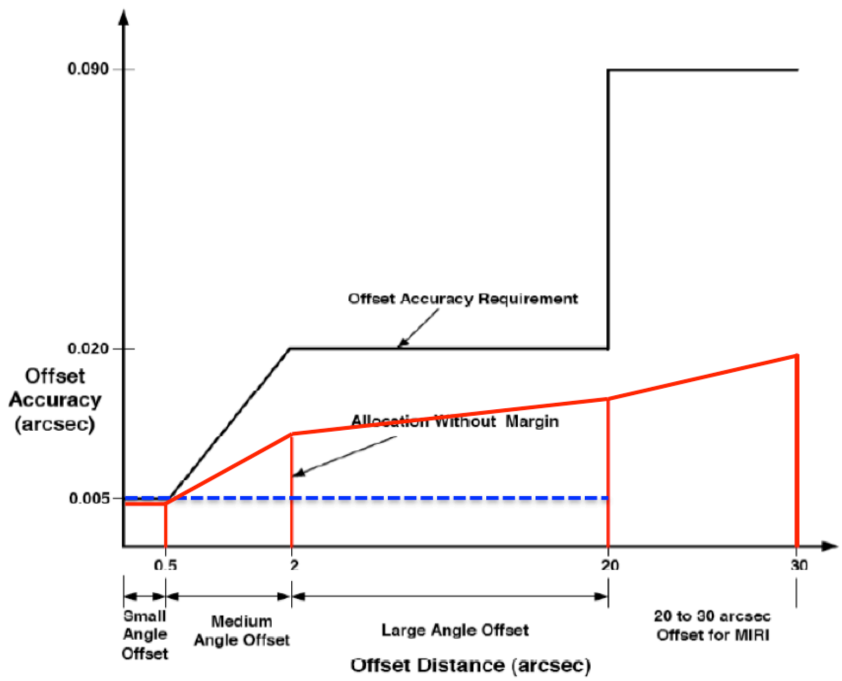

Figure 1: Slew accuracy as a function of slew size. We use different slew accuracies to estimate their contribution to final pointings. Models are Requirement (*black*), Intermediate (*red*) and January 2014 Spacecraft Critical Design Review (CDR)(*blue*).

3 Simulations

As described in Lajoie et al. (2013), our simulations involve the creation of MIRI coronagraphic PSFs and their manipulation to model various noise sources and detector artifacts. We include the transmission profiles for the 4QPM and the coronagraphic filter, as well as the detector quantum efficiency. Moreover, we add stellar and background photon noise sources, detector readout noise, and pixel-to-pixel variations to our images. Latency is modeled with a simple prescription using 1% of the previous image with an exponential decay timescale of 300 seconds. At the time of this report (and when the simulations were run), these numbers were assumed more or less accurate, although not necessarily based on extensive MIRI detector characterization. Recent work by Greene & Walker (2013) suggest that the initial latent amplitude is below 1% and that it decays more rapidly, on the order of 10 seconds. The fact that latent images are fainter and faster-decaying will clearly help improve the contrast performances of the coronagraphs. However, since we assume the same latency prescription as in papers 2 and 3 (Lajoie et al. 2012, 2013), the reader should view the results presented here as "worst-case scenario" as far as latency is concerned and any prescription that has smaller amplitude and shorter timescale will only work in our favor. No image drift or jitters were included in our simulations of target acquisition, although Soummer et al. (2013) showed that these effects have only minor impact on TA under the REQ assumption for the SAMs. For a more detailed discussion of our simulations, refer to Soummer et al. (2010), and Lajoie et al. (2012, 2013).

Target acquisition is usually performed with the neutral density filter (FND) using a pre-defined scenario (see Figure 2). We simulate latency for assessing contrast performances by assuming that the slew(s) from the TA location to the center of the 4QPM are performed with the opaque filter in place, and that the filter wheel is rotated from the opaque filter to the desired coronagraphic filter (with light continuously falling on the detector) once the star is located on the coronagraphic mask. As discussed earlier, the effect of latents on both target acquisition and contrast performance was found to be negligible after 10,000 seconds by Lajoie et al. (2012, 2013), assuming a simple prescription for latency. We nevertheless include it here for completeness.

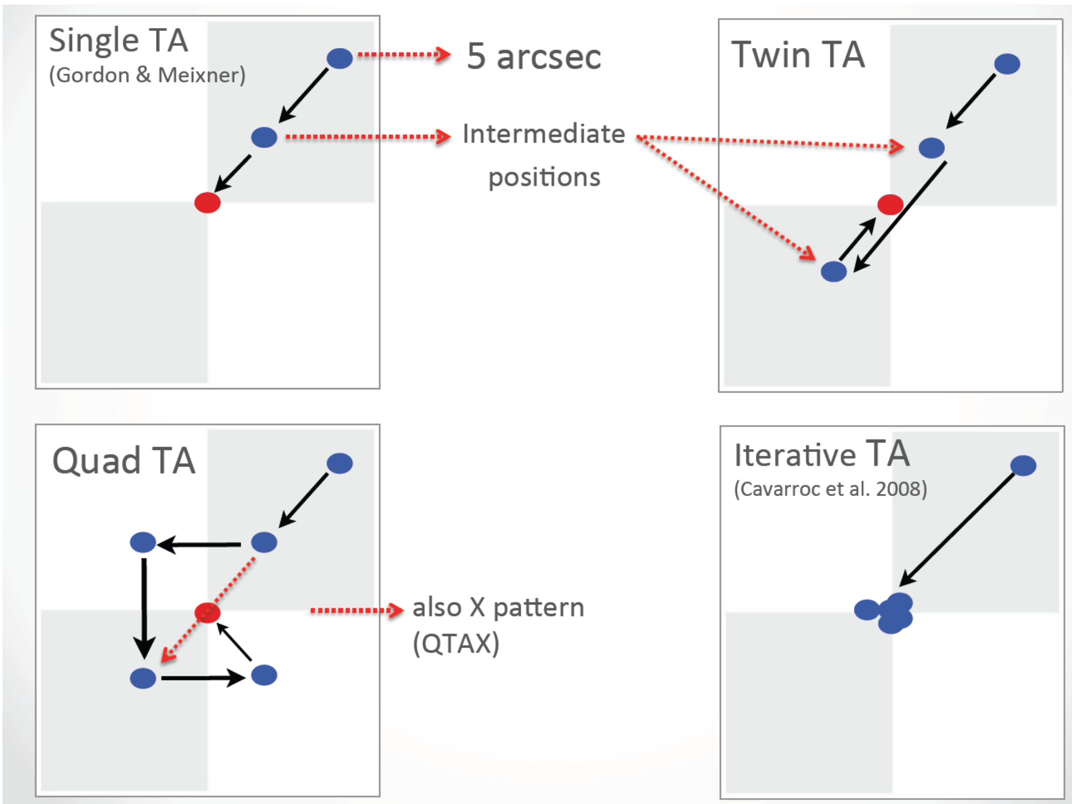

Figure 2 Various target acquisition scenarios discussed in this report. The accuracy of each scenario was investigated by Lajoie et al. (2012).

4 Results for Different Slew Accuracy Models

In this report, we summarize and assess the 4QPM coronagraphs pointing and contrast performances separately. We define the "contrast" as the mean radial intensity normalized to the peak off-axis coronagraphic PSF (in other words, the PSF without the 4QPM), and with reference star subtraction. Note that while this definition of contrast is a common metric used in coronagraphy, it does not correspond to a detection sensitivity of actual astrophysical objects. For a detailed description and treatment of detection sensitivity, see ETC coronagraphy estimates by Pueyo et al. (2014).

First, we discuss the three slew accuracy models separately and report their respective performances in a consistent manner to allow for quick comparisons. In particular, as in Lajoie et al. 2012, we report the final pointings dispersion and mean offset as a metric for assessing the performances of a slew model as well as whether these numbers meet the specified requirements. Our main findings are summarized in Table 1, where we use the following color code: Green: meets coronagraphic requirements; Yellow: marginal; Red: does not meet coronagraphic requirements. Following on Cavarroc et al. (2008) the MIRI coronagraphic requirement of the 4QPM were defined as 5 mas maximum offset between star and reference and 10 mas maximum offset between target star and center of the mask. Finally, we remind the reader that Lajoie et al. (2012) showed the accuracy of centroid measurement during target acquisition to be independent of wavelength (unlike the contrast performances). Our assessment of target acquisition performance therefore applies to all wavelengths, whereas the contrast performances are reported at all 4QPM wavelengths.

Case 1: Slews based on Requirement model (REQ)

In general, we find that the target acquisition under the REQ slew accuracy model is most accurate for slews of ~500 mas. There are no gains in accuracy for smaller slews because adverse effects of the 4QPM closer to the apex become important and make centroid measurements much less accurate. We therefore do not recommend performing target acquisition within 500 mas of the 4QPM center and no further than ~750 mas. However, performing target acquisition at such small separations poses serious concerns for potential latent images in the science image since these angular separations overlap with prime science for planet direct imaging.

Case 2: Slews based on Intermediate model (INT)

The INT case was previously discussed and used by Lajoie et al. (2012, 2013), which they referred to as EXP. Similarly to the REQ case discussed above, the Intermediate case has its smallest slew error for slews smaller than 500 mas. If the INT model turns out to be valid, we therefore recommend performing target acquisition around 500 mas in order to achieve final pointings as close to the center of the 4QPM as possible. Again, we emphasize however that performing target acquisition around 500 mas might imprint latent images on the science observations. In the REQ and INT cases, the user will therefore have to compromise pointing accuracy with possible latent images overlapping science targets.

Case 3: Slews based on S/C-CDR model (CDR)

The S/C-CDR slew accuracy model is flat at 5 mas (1-sigma/axis) all the way to 20”, and as such, yields the best target acquisition performances. For slews smaller than 20”, the 4QPM contrast performances are minimally limited by the final slew to the center and provide the advantage of being able to perform TA as far as possible from the center of the 4QPM and therefore minimize the impact of any latent images on the science images.

Table 1 Summary of our simulations results allowing for quick assessment of predicted pointing performances of MIRI 4QPM coronagraphs based on the observatory's slew accuracy model. Green meets the requirements; Yellow is marginal; Red does not meet the requirements.

Slew Accuracy	Best pointing performances			
	TA Method	Δ pos (mas)	σ (mas)	Offset (mas)
REQ	S-TA	500	8	7
	T-TA	500	17	5
	Q-TA	500	13	4
	Q-TAX	500	20	2

Slew Accuracy	Best pointing performances			
	TA Method	Δ pos (mas)	σ (mas)	Offset (mas)
INT	S-TA	500	6	7
	T-TA	500	11	4
	Q-TA	500	9	4
	Q-TAX	500	13	2

Slew Accuracy	Best pointing performances			
	TA Method	Δ pos (mas)	σ (mas)	Offset (mas)
CDR	S-TA	> 4000	7	7
	T-TA	> 4000	8	4
	Q-TA	> 4000	8	4
	Q-TAX	> 4000	9	2

Table 1 clearly shows that the Single TA scenario consistently yields the best pointing performances for all three slew accuracy models used. The other scenarios yield pointings that marginally meet the goals, even for the best slew accuracy model. *We emphasize in particular that the REQ slew accuracy model also do not yield pointings that meet the requirements for any of our target acquisition scenario.*

Based on the pointing accuracy results of Table 1, we show in Figure 3 the contrast curves at all wavelengths and for all three SAM accuracy models based on the Single TA scenario only. The Single TA scenario was shown to yield the best pointings for all the slew accuracy models. The contrast curves of Figure 3 were derived using all combinations of target and reference from 50 random pointings (shown in the insets), which were generated using one of the slew accuracy models (see label on left) as well as an approach similar to the Single TA scenario. PSFs were generated for each of these pointings and scaled for magnitude 6 and 4 (target and reference respectively), including latency and all sources of noise (see Lajoie et al. 2013 for more information). The dashed contrast curve shows the average contrast where the red lines delineate the +/- 1-sigma standard deviation.

Figure 3 shows that the effect of slew accuracy is most obvious at the peak of the curves and, to a lesser extent, in the 1-sigma spread around the average curve (dashed line). Indeed, for any given wavelength, a better slew accuracy (e.g. going from REQ to INT to CDR) will improve the contrast by almost an order of magnitude. On the other hand, the effect of wavelength is also obvious as the 4QPM at 15.50 μm is always mostly limited by the background photon noise. For that reason, we see no improvement in contrast at large angular separations for the INT or CDR slew accuracy models. As pointed out by Lajoie et al. (2013), the largest limiting factor in our simulations was found to be the background photon noise, which is also more dominant at longer wavelength. The arrows represent the background level, as determined from a simple average of the corner of our contrast images. It is interesting to note that the envelope of the contrast curves for FQPM 1065 reaches the background level at approximately 16 λ/D, whereas the contrast curves of FQPM 1550 reach the background level at only 6-7 λ/D.

In general, our results show that the contrast requirement (2.5×10^{-5} at 10 λ/D) can be met only in the INT and CDR slew accuracy models. *The REQ slew accuracy model does not yield contrast at 10 λ/D that meet the requirement defined in §2.*

We also summarize our results in Table 2 as an aid to the reader when trying to estimate the expected performances of a coronagraph at a given wavelength under a given slew accuracy model. Note that because the REQ and INT slew models have their smallest slew errors within 500 mas, the potential of having strong latents is also largest; the last column of Table 2 reminds the reader of that eventuality.

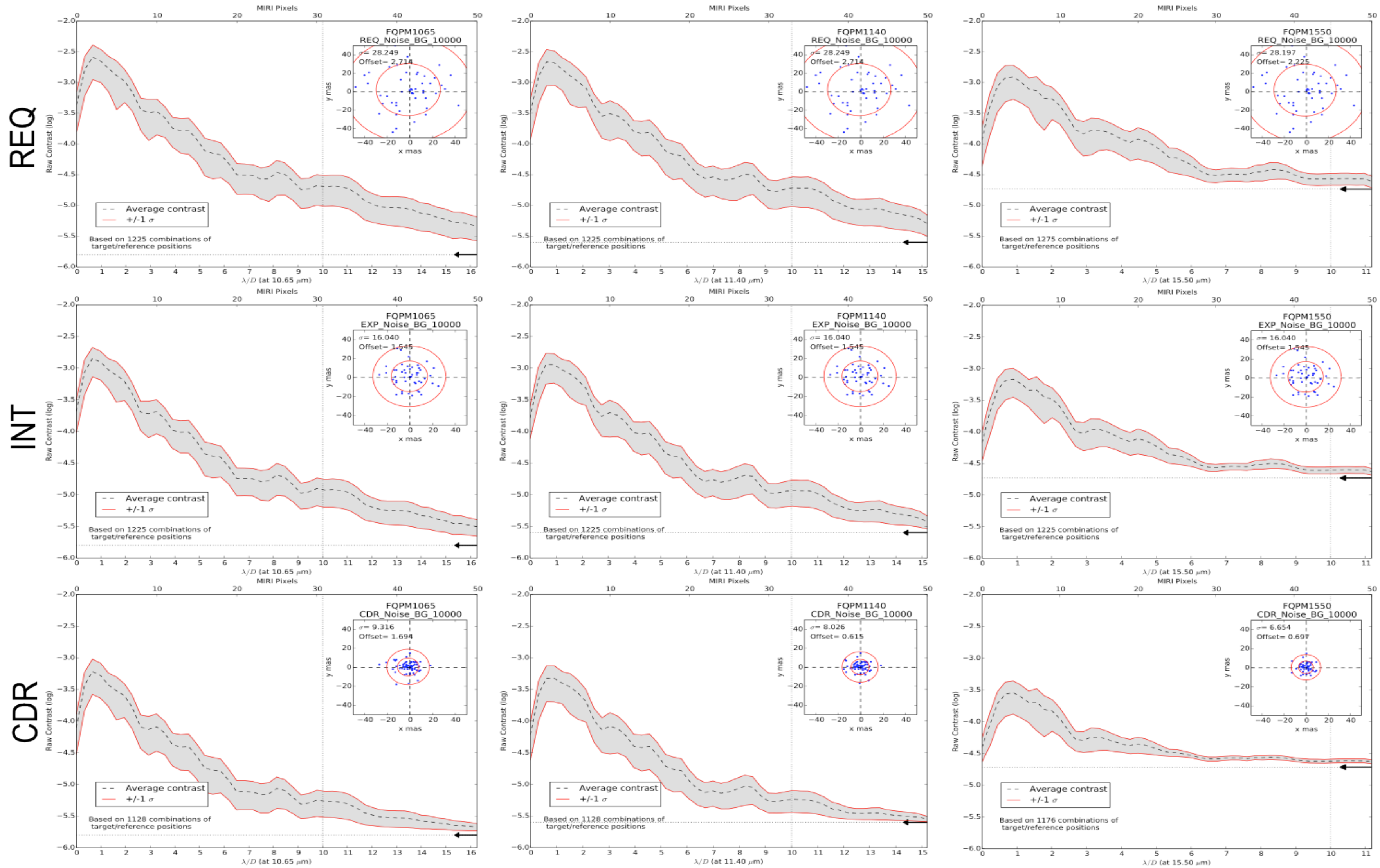

Figure 3: Contrast after 10,000 seconds in the 10.65, 11.40, and 15.50 um 4QPM (left to right respectively) for targets and references of magnitudes 6 and 4 respectively, including noise. The three slew accuracy models are shown on different rows. The dashed line shows the average of ~1200 contrast curves whereas the red lines show the +/- 1 sigma standard deviation. The top and bottom x-axis show the size of MIRI pixels and the corresponding scale in λ /D respectively. The insets show the Single TA random pointings generated to derive the average contrast curves (see also Lajoie et al. 2013). The arrows show the approximate background level.

Table 2 Summary of our simulations results allowing for quick assessment of predicted contrast performances of MIRI 4QPM coronagraphs based on the observatory's slew accuracy. The contrast numbers shown here were derived using the Single TA scenario slewing from a 2-arcsecond intermediate position. The color code is the same as Table 1, where the requirement at 10 λ/D is of 2.5×10^{-5} (log -4.6). Note that there are no performance goals at smaller angular separations.

Slew Accuracy	λ (µm)	Log (Contrast)		Risk of Latents on Science?
		1 λ/D	10 λ/D	
REQ	**10.65**	-2.60	-4.75	Y
	11.40	-2.60	-4.75	Y
	15.50	-3.00	-4.50	Y

Slew Accuracy	λ (µm)	Log (Contrast)		Risk of Latents on Science?
		1 λ/D	10 λ/D	
INT	**10.65**	-2.80	-5.00	Y
	11.40	-2.80	-5.00	Y
	15.50	-3.25	-4.60	Y

Slew Accuracy	λ (µm)	Log (Contrast)		Risk of Latents on Science?
		1 λ/D	10 λ/D	
CDR	**10.65**	-2.75	-5.25	N
	11.40	-2.75	-5.25	N
	15.50	-3.50	-4.60	N

5 Conclusions

We presented the results of large-scale coronagraphic simulations aimed at optimizing both the target acquisition as well as the performances of the four-quadrant phase mask coronagraphs on MIRI. The summary provided here allows the user to optimize the coronagraphs operations based on various observatory slew accuracy models. Based on mean offset and dispersion, our results suggest that the single TA scenario performs the best. Our simulations further show that the slew model with the highest accuracy (i.e. from the January 2014 S/C-CDR) provides (1) the best pointing performances as well as (2) the best contrast performances at all wavelengths, although the background photon noise constitutes a limiting factor at longer wavelengths. These results are now being implemented into the MIRI operations concept document (OCD; see Hines et al. 2014) and should be used as estimates for the expected performance of the MIRI 4QPM coronagraphs.

6 References

- Cavarroc, C., Boccaletti, A., Baudoz, P., Amiaux, J., & Regan, M. 2008, *Target Acquisition for MIRI Coronagraph*. PASP 120, pp1016-1027
- Greene, T. & Walker H. 2013, MIRI team technical report, MIRI-TN-00001-ARCDetector-Latent-Correction
- Hines, D.C., Lajoie, C-P, & Soummer, R. 2014, JWST-STScI Technical Reports, in preparation.
- Lajoie, C-P, Soummer, R., & Hines D. 2012, *Simulations of Target Acquisition with MIRI Four-Quadrant Phase Mask Coronagraph (II)*. STScI JWST Technical Reports JWST-STScI-003065, SM-12
- Lajoie, C-P, Soummer, R., & Hines D. 2013, *Simulations of MIRI Four-Quadrant Phase Mask Coronagraph (III) Target Acquisition and CCC mechanism Usage*. STScI JWST Technical Reports, JWST-STScI-003546, SM-12
- Pueyo et al. 2014, STScI Technical Report, in preparation.
- Soummer, R., & Makidon, R, P. 2010, *Simulations of MIRI coronagraphic images*, STScI Technical Report, JWST-STScI-001952, SM-12
- Soummer, R., Hines, D., & Marshall, P. 2013, *Simulations of Target Acquisition with MIRI Four-Quadrant Phase Mask Coronagraph (I),* STScI Technical Report, JWST-STScI-003063, SM-12